Published in final edited form as:
Nat Biotechnol. 2004 January ; 22(1): 93–97.

Near-infrared fluorescent type II quantum dots for sentinel lymph node mapping

Sungjee Kim[1,6], **Yong Taik Lim**[2,5,6], **Edward G Soltesz**[3], **Alec M De Grand**[2], **Jaihyoung Lee**[2], **Akira Nakayama**[2], **J Anthony Parker**[4], **Tomislav Mihaljevic**[3], **Rita G Laurence**[3], **Delphine M Dor**[3], **Lawrence H Cohn**[3], **Mounqi G Bawendi**[1], and **John V Frangioni**[2,4]

1*Department of Chemistry, Massachusetts Institute of Technology, Cambridge, Massachusetts 02139, USA*

2*Division of Hematology/Oncology, Department of Medicine, Beth Israel Deaconess Medical Center, Boston, Massachusetts 02215, USA*

3*Division of Cardiac Surgery, Department of Surgery, Brigham and Women's Hospital, Boston, Massachusetts 02115, USA*

4*Department of Radiology, Beth Israel Deaconess Medical Center, Boston, Massachusetts 02215, USA*

Abstract

The use of near-infrared or infrared photons is a promising approach for biomedical imaging in living tissue[1]. This technology often requires exogenous contrast agents with combinations of hydrodynamic diameter, absorption, quantum yield and stability that are not possible with conventional organic fluorophores. Here we show that the fluorescence emission of type II[2,3] quantum dots can be tuned into the near infrared while preserving absorption cross-section, and that a polydentate phosphine coating renders them soluble, disperse and stable in serum. We then demonstrate that these quantum dots allow a major cancer surgery, sentinel lymph node mapping[4–6], to be performed in large animals under complete image guidance. Injection of only 400 pmol of near-infrared quantum dots permits sentinel lymph nodes 1 cm deep to be imaged easily in real time using excitation fluence rates of only 5 mW/cm^2. Taken together, the chemical, optical and *in vivo* data presented in this study demonstrate the potential of near-infrared quantum dots for biomedical imaging.

We prepared near-infrared (NIR) type II quantum dots (QDs) (see Supplementary Fig. 1 online) with an oligomeric phosphine coating[7] that rendered them soluble in aqueous buffers (see Methods and Supplementary Fig. 1 online). When sterile-filtered and stored as a 2- to 4-μM stock solution in phosphate-buffered saline (PBS), NIR type II QDs remained stable for at least four weeks at room temperature. Transmission electron microscopy (TEM) of NIR type II QDs dispersed in water showed fairly spherical semiconductor particles 10 nm in diameter (Fig. 1a). Using a model described earlier by our group[1], we chose NIR emission wavelengths that offset the competing effects of tissue photon penetration and charge-coupled device (CCD) camera quantum efficiency. In neutral aqueous buffer, the peak emission was tuned to 840–860 nm while preserving absorption cross-section (Fig. 1b and Supplementary Fig. 1 online). The full-width half-maximum of the emission was 90 nm. NIR QDs showed typical broadband

Correspondence should be addressed to J.V.F. (jfrangio@bidmc.harvard.edu).
[5]Present address: Electronics and Telecommunications Research Institute, 161 Gajeong-dong, Yuseong-gu, Daejeon, 305–350, Republic of Korea.
[6]These authors contributed equally to this study.

Note: Supplementary information is available on the Nature Biotechnology website.

COMPETING INTERESTS STATEMENT
The authors declare that they have no competing financial interests.

absorption, with an increasing extinction coefficient at bluer wavelengths (Fig. 1b). At the first absorption peak (775 nm), the extinction coefficient was 580,000 $M^{-1}cm^{-1}$ (Fig. 1b), consistent with the large particle size. The quantum yield in PBS was 13% (data not shown). By gel filtration, NIR QDs ran equivalently to a protein of 440 kDa. This corresponds to a hydrodynamic diameter of approximately 15.8 nm (Fig. 1c), which is well within the critical hydrodynamic diameter range of 5–50 nm needed for retention of QDs in the sentinel lymph node (SLN)[8]. The hydrodynamic diameter measured by quasi-elastic light scattering (QELS) was 18.8 nm (data not shown). Our data suggest that polydentate phosphines add a minimal thickness to the QD as the hydrodynamic diameter measured by both gel filtration and QELS was only 5.8–8.8 nm larger than the diameter of the inorganic core and shell measured by TEM.

Conventional NIR fluorophores, such as IRDye78-CA, dissolved in serum or aqueous buffer rapidly photobleach when exposed to fluence rates above their photobleaching threshold (Fig. 1d; ref. [9]). In contrast, NIR QDs coated with oligomeric phosphines actually photobrighten slightly as fluence rate increases and show no deterioration of fluorescence emission even at fluence rates of 600 mW/cm^2 (Fig. 1d). Photobrightening effects have been observed previously in similar systems[10,11]. The mechanism is postulated to be either a photoannealing effect or a photoneutralization effect. We further assessed the serum stability of NIR QDs by incubating them in 100% serum at 37 °C and recovering them by filtration. After 30 min (twice as long as a typical SLN mapping procedure), total fluorescence emission decreased by only 10%, indicating minimal aggregation and/or reduction of fluorescence quantum yield (Fig. 1e). These data suggest that type II NIR QDs will perform well in biomedical applications, such as SLN mapping, under conditions of high fluence rate and prolonged exposure to bodily fluids at core body temperature.

The type II NIR QDs described in this study were engineered with a hydrodynamic diameter of 15–20 nm, a maximal absorption cross-section, fluorescence emission at 840–860 nm, a reasonable aqueous quantum yield and a stable organic coating. Because of their optimal size for retention in lymph nodes, we explored whether these QDs could be used for lymphatic mapping. When injected intradermally in the paw of a mouse ($n = 4$), NIR QDs entered the lymphatics and migrated within minutes to an axillary location that could be detected using our previously described intraoperative imaging system[12] (Fig. 2a). Reinjection of the same site with the gold-standard SLN mapping agent isosulfan blue resulted in colocalization of the NIR fluorescence signal and the blue dye (Fig. 2b) in what was confirmed histologically to be the SLN (data not shown).

These mouse data are relevant to axillary SLN mapping for diseases such as breast cancer; however, we wanted to prove that NIR QDs could be used in large animals the size of humans. We found that when 400 pmol of NIR QDs were injected intradermally on the thigh of a 35 kg pig ($n = 5$), a surgeon was able to follow lymphatic flow towards the SLN in real time and to quickly identify the position of the SLN (Fig. 2c). These real-time images included lymph channels that diverge from the injection site and then coalesce into the SLN (Fig. 2c). Localization of the SLN required only 3–4 min, and the NIR QDs permitted image guidance throughout the procedure. Indeed, such guidance minimized the size of the incision needed to find the node, because its position could be determined beforehand, and as tissue was dissected, the intensity of the SLN increased exponentially (Fig. 2c). This removed all ambiguity about SLN location and permitted identification of the SLN even when it was part of a large lymph node cluster (see below), as is common in pigs. As was seen in the mouse, coinjection of isosulfan blue resulted in colocalization of NIR fluorescence and dye (Fig. 2c). The average depth of the femoral SLN in the pig was approximately 1 cm from the skin surface and, as determined by fluorescence, approximately 2–4% of the injected dose accumulated in the SLN (data not shown). After the procedure, the surgical site was inspected with high sensitivity to ensure complete resection of the SLN (Fig. 3a). Analysis of resected tissue showed that NIR

QDs were completely trapped in the SLN (Fig. 3a) and confined to the outermost rim of the node (Fig. 3b,c). These data are consistent with the known sieving properties of the lymph node's subcapsular sinus.

We have demonstrated that type II NIR QDs with a polydentate phosphine coating can be used effectively for SLN mapping in both small and large animals. These data are significant for several reasons. First, NIR QDs eliminate the need for both a radioactive tracer and a blue dye, because lymph flow and the SLN can be identified optically, and in real time, using intraoperative NIR fluorescence imaging. Second, the surgeon is provided with image guidance, including imaging of underlying anatomy, throughout the procedure. At present, the learning curve for SLN mapping is several dozen cases. NIR QDs have the potential to markedly improve this learning curve. Third, after resection, the surgeon can inspect the surgical site with high sensitivity to ensure completeness of the procedure. Fourth, the pathologist can easily identify the SLN after resection, even if it is part of a large nodal chain (Fig. 3a) or matted to other bloody tissue, and can focus attention on the specific part of the SLN that is most likely to contain malignant cells. Fifth, unlike small molecules such as isosulfan blue, NIR QDs have an optimal size (and thus do not flow past the SLN), have a maximal absorption cross-section and do not photobleach.

It should be emphasized that our large-animal studies were performed with only 5 mW/cm^2 of NIR excitation light and 400 pmol of NIR QDs. Despite this low fluence rate, we were able to identify SLNs approximately 1 cm below the skin surface using reflectance imaging. Our data suggest that even higher sensitivity can be achieved without concern for photobleaching. Optical guidance, even in bloody surgical fields, is likely to permit SLN mapping of other human cancers, such as colon cancer, which until now has been technically difficult. Additionally, frequency-domain photon migration techniques[13,14] will likely extend depth detection to the 6- to 10-cm range.

The toxicity of NIR QDs has not yet been examined. In their elemental form, the three metals (cadmium, tellurium and selenium) have known acute and chronic toxicities. However, no data exist on the toxicity of precomplexed nanocrystals injected subdermally. Without such data, one can only speculate by extrapolating the known dose-effect relationships for oral exposure. For the pig experiments described above, 400 pmol of NIR QDs corresponds to approximately 9.9 μg/kg, 7.3 μg/kg, 2.4 μg/kg and 4.1 μg/kg of cadmium, telluride, selenide and alkyl phosphines, respectively. In the case of cadmium, for which the most data are available, this dose is approximately 300 times lower than the daily dose that causes renal toxicity in rats after 6 weeks of continuous exposure in drinking water[15]. Moreover, a treatment for elemental cadmium poisoning in humans is the infusion of elemental selenium to produce less toxic cadmium selenide salts. It is possible, therefore, that despite being composed of potentially toxic materials, the low dose and chemical form of the materials are such that the overall toxicity is low. In the short term, at least, we saw no change in electrocardiographic and pulse oximetry measurements during large-animal surgery and for several hours thereafter.

Our data suggest simple strategies for minimizing the potential for toxicity. The first is simply to increase the fluence rate and proportionally lower the injected NIR QD dose. The photobleaching data suggest that at least a 100-fold lower dose could be used. The second is that type II structures permit combinations of nontoxic materials, which would otherwise emit in the visible light range, to emit in the NIR. Finally, during a typical SLN mapping procedure, the tumor (site of QD injection) and SLN are both resected, thus minimizing exposure to the QD materials. Future studies should address these important issues and the use of type II QD structures in other biomedical assay and imaging applications.

Because of their unique optical properties, type II NIR QDs provide the surgeon with direct visual guidance throughout the entire SLN mapping procedure, minimize incision and dissection inaccuracies, and permit real-time confirmation of complete resection. SLN mapping has already revolutionized cancer surgery. The technology described in this study has the potential to improve the technique even further.

METHODS

Animals

Animals were used in accordance with approved institutional protocols from the BIDMC and BWH. SKH1 mice were from Charles River Labs. Yorkshire pigs (35 kg) were from EM Parsons. Mice were anesthetized with 50 mg/kg intraperitoneal pentobarbital. Pigs were induced with 4.4 mg/kg intramuscular Telazol (Fort Dodge Labs) and anesthesia was maintained through a 7-mm endotracheal tube with 1.5% isoflurane/98.5% O_2 at 5 l/min.

Reagents

Isosulfan blue (1%) was from US Surgical. Oxazine 725 was from Exciton. IRDye78-CA was a generous gift from LI-COR. Trioctylphosphine oxide (TOPO), selenium shot and tellurium shot were from Alfa Aesar. Trioctylphosphine (TOP) was from Fluka. Diisocyanatohexane and ethylisocyanatoacetate (EIA) were from Aldrich. Gel-filtration standards were from Sigma. Dimethylcadmium and trishydroxypropylphosphine were from Strem. All other reagents were from Fisher Scientific.

Preparation of NIR CdTe(CdSe) core(shell) type II QDs

All procedures were performed under an inert atmosphere, as described previously[1], unless otherwise specified. CdTe QDs[16] and bis(trimethylsilyl)selenide (BTS)[17] were synthesized as described previously. QDs were precipitated by centrifuging at 6,000*g* for 10 min in methanol.

Precipitated CdTe QDs were dispersed in a mixture of 15 g TOPO and 5 ml TOP, and dried under vacuum at 140 °C for 3 h. An over-coating stock solution was prepared by mixing 1:1 molar stoichiometry of dimethylcadmium and BTS in TOP. While the CdTe QD solution in TOPO and TOP was vigorously stirred at 100 °C, over-coating solution was added dropwise, then the mixture was stirred an additional 3 h at 100 °C. The reaction temperature was raised to 200 °C and stirring was continued until the desired wavelength was obtained by optical spectroscopy (Ocean Optics S2000). Shell formation proceeded by fusion of small particles of CdSe onto the cores, as well as by Ostwald ripening, and required several days to complete.

Oligomeric phosphine organic coating

First, 8 g trishydroxypropylphosphine was dissolved in 20 g dimethylformamide (DMF) and stirred vigorously at room temperature. Diisocyanatohexane (4.5 g) was added dropwise and stirred for 1 d. EIA (19.4 g) was added dropwise and stirred overnight. Solvent and excess EIA were removed at 100 °C under vacuum.

For cap exchange, 100 mg of precipitated QDs was mixed with 3.0 g oligomeric phosphine ligands in 10 ml tetrahydrofuran (THF) and 2 ml DMF and stirred at room temperature for 1 h; then THF and DMF were removed at 100° C under vacuum. The resultant viscous mixture was incubated at 120° C for 3 h and then cooled to room temperature. Next, 50 ml of 1 N NaOH was added, forming a two-phase suspension, and the solution was stirred vigorously at room temperature until only a single, slightly turbid dark brown solution was present. The solution was filtered through a 0.2-μM PTFE filter (Nalgene) and then ultrafiltered with 1,000 volumes of PBS, pH 7.4, using a 50-kDa-cutoff membrane (Pellicon XL, Millipore).

NIR QD characterization

The total mass per QD particle was measured by dividing the inorganic mass per particle, as measured by TEM, by the mass of inorganic cores in a dried QD sample, as measured using a Seiko thermogravimetric analyzer. Absorbance and photoluminescence were measured on a HP-8453 spectrophotometer (Hewlett-Packard) and SPEX Fluorolog-2 spectrofluorometer (Jobin Yvon Horiba), respectively. Photobleaching was done with a 770-nm laser diode[9]. For serum stability, NIR QDs were filtered through a 0.2-μm filter before fluorescence measurements (500 nm excitation, 850 nm emission). Quantum yield was measured using oxazine 725 in ethylene glycol as a standard. Gel-filtration chromatography was performed on a Biologics LP system (Bio-Rad) using Sephacryl S-400 resin (Sigma) and an XK 16/20 column (Amersham) at a linear flow rate of 15 cm/h. Column height was 6.5 cm. QELS was performed on a Model 90 Plus particle size analyzer (Brookhaven Instruments) with ZetaPALS particle sizing software version 2.32.

Sentinel lymph node identification

For mouse experiments, 10 μl of either 1 μM NIR QDs in PBS, pH 7.4, or 1% (17.6 mM) isosulfan blue was injected intradermally into the paw. For pig experiments, 200 μl of either 2 μM NIR QDs in PBS, pH 7.4, or 1% (17.6 mM) isosulfan blue was injected intradermally into the thigh. For histology, OCT-embedded tissue was cryo-sectioned at 6 μm onto Superfrost Plus slides.

Intraoperative NIR fluorescence imaging

The intraoperative NIR fluorescence imaging system was as described previously[12], except the 770-nm laser was replaced with two 150-W halogen sources with 725- to 775-nm bandpass filters (Chroma), a 795-nm longpass emission filter (Chroma) was used, and system control was done with LabVIEW (National Instruments)[18]. The field of view was 20 cm in diameter. Fluence rates for white light (400–700 nm) and NIR excitation light were 2 mW/cm^2 and 5 mW/cm^2, respectively. Exposure times were 33 ms and 67 ms for color video and NIR fluorescence images, respectively.

Supplementary Material

Refer to Web version on PubMed Central for supplementary material.

Acknowledgements

We thank Grisel Rivera for administrative assistance and Daniel A. Brown (BIDMC) for frozen sectioning. This work was supported by the Post-Doctoral Fellowship Program of the Korea Science and Engineering Foundation (KOSEF; Y.T.L.). This work was also supported in part by the US National Science Foundation–Materials Research Science and Engineering Center program under grant DMR-9808941 (M.G.B.), the US Office of Naval Research (M.G.B.), the Stewart Trust of Washington, D.C. (J.V.F.), US Department of Energy (Office of Biological and Environmental Research) grant DE-FG02-01ER63188 (J.V.F.) and US National Institutes of Health grant R21 EB-00673 (J.V.F. and M.G.B.).

References

1. Lim YT, et al. Selection of quantum dot wavelengths for biomedical assays and imaging. Mol Imaging 2003;2:50–64. [PubMed: 12926237]
2. Hatami F, et al. Carrier dynamics in type-II GaSb/GaAs quantum dots. Phys Rev B 1998;57:4635–4641.
3. Kim S, Fisher B, Eisler HJ, Bawendi M. Type-II quantum dots: CdTe/CdSe(core/shell) and CdSe/ZnTe (core/shell) heterostructures. J Am Chem Soc 2003;125:11466–11467. [PubMed: 13129327]
4. Jakub JW, Pendas S, Reintgen DS. Current status of sentinel lymph node mapping and biopsy: facts and controversies. Oncologist 2003;8:59–68. [PubMed: 12604732]

5. Bonnema J, Van DVCJ. Sentinel lymph node biopsy in breast cancer. Ann Oncol 2002;13:1531–1537. [PubMed: 12377640]
6. Thompson JF, Uren RF. Lymphatic mapping and sentinel node biopsy for melanoma. Expert Rev Anticancer Ther 2001;1:446–452. [PubMed: 12113111]
7. Kim S, Bawendi MG. Oligomeric ligands for luminescent and stable nanocrystal quantum dots. J Am Chem Soc. 2003in the press
8. Uren, RF.; Hoefnagel, CA. Textbook of Melanoma. Thompson, JF.; Morton, DM.; Kroon, BBR., editors. Chapter 30. Martin Dunitz; London: 2003.
9. Nakayama A, Bianco AC, Zhang CY, Lowell BB, Frangioni JV. Quantitation of brown adipose tissue perfusion in transgenic mice using near-infrared fluorescence imaging. Mol Imaging 2003;2:37–49. [PubMed: 12926236]
10. Manna L, Scher EC, Li LS, Alivisatos AP. Epitaxial growth and photochemical annealing of graded CdS/ZnS shells on colloidal CdSe nanorods. J Am Chem Soc 2002;124:7136–7145. [PubMed: 12059239]
11. Wang Y, Tang Z, Correa-Duarte MA, Liz-Marzan LM, Kotov NA. Multicolor luminescence patterning by photoactivation of semiconductor nanoparticle films. J Am Chem Soc 2003;125:2830–2831. [PubMed: 12617622]
12. Nakayama A, del Monte F, Hajjar RJ, Frangioni JV. Functional near-infrared fluorescence imaging for cardiac surgery and targeted gene therapy. Mol Imaging 2002;1:365–377. [PubMed: 12940233]
13. Ntziachristos V, Bremer C, Weissleder R. Fluorescence imaging with near-infrared light: new technological advances that enable *in vivo* molecular imaging. Eur Radiol 2003;13:195–208. [PubMed: 12541130]
14. Sevick-Muraca EM, Houston JP, Gurfinkel M. Fluorescence-enhanced, near infrared diagnostic imaging with contrast agents. Curr Opin Chem Biol 2002;6:642–650. [PubMed: 12413549]
15. US Department of Energy. Risk Assessment Information System. http://risk.lsd.ornl.gov/tox/rap_toxp.shtml
16. Mikulec, FV. Ph D Thesis. Department of Chemistry, Massachusetts Institute of Technology; Cambridge Massachusetts USA: 1999. Semiconductor nanocrystal colloids: manganese doped cadmium selenide, (core)shell composites for biological labeling, and highly fluorescent cadmium telluride.
17. Drew MGB, Rice DA, Williams DM. Synthesis of Nb(O2H5C7)3Y (Y = O, S and Se): crystal structure of oxotris (tropolonato) niobium(V) monohydrate: a seven coordinate monomer containing a terminal Nb:O bond. Inorgan Chim Acta 1986;118:165–168.
18. De Grand AM, Frangioni JV. An operational near-infrared fluorescence imaging system prototype for large animal surgery. Technol Cancer Res Treat. 2003in the press

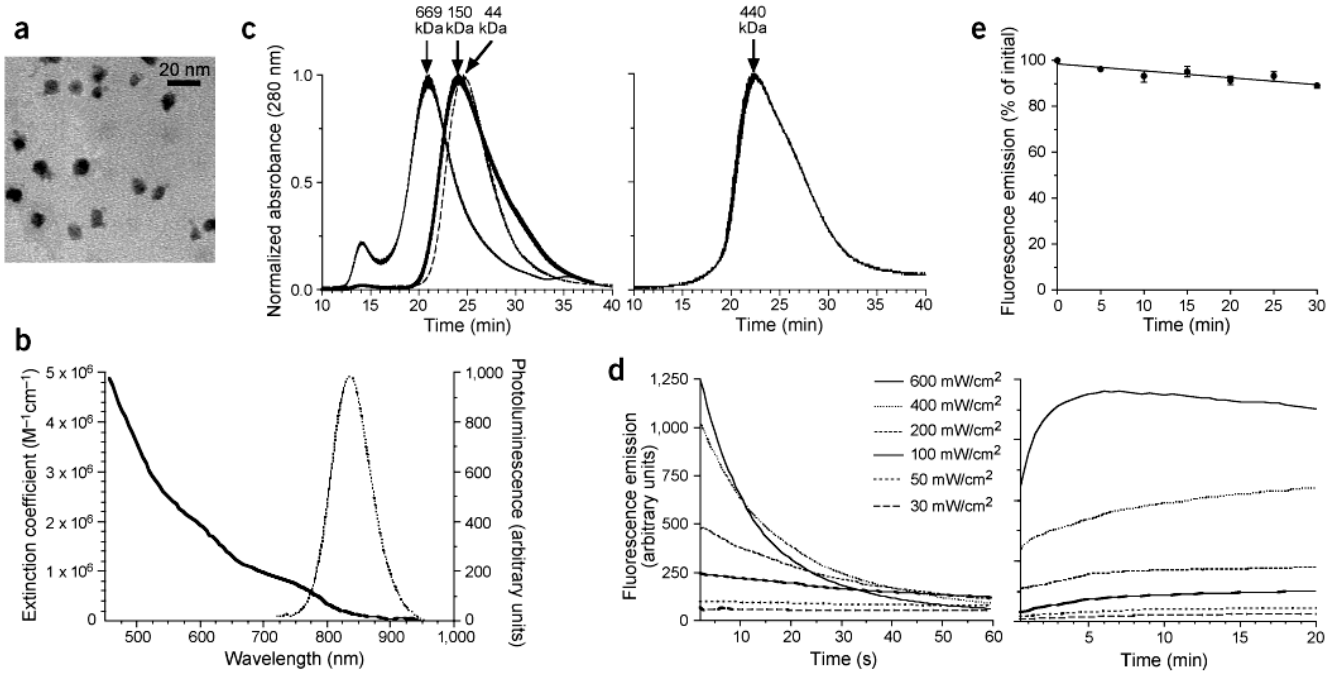

Figure 1.

Physical and optical properties of aqueous-soluble, NIR type II QDs. (**a**) TEM image of water-dispersed NIR QDs. (**b**) Molar extinction coefficient (solid curve; left axis) and photoluminescence intensity (dashed curve; right axis) of NIR QDs in PBS, pH 7.4. (**c**) Gel-filtration chromatography of protein standards (left) and NIR QDs (right) in PBS, pH 7.4. Standards included thyroglobulin (669 kDa; solid curve), alcohol dehydrogenase (150 kDa; thick solid curve) and ovalbumin (44 kDa; dotted curve). NIR QDs had an effective molecular weight of 440 kDa. (**d**) Fluorescence stability of 1 μM organic NIR fluorophore IRDye78-CA (left) and 1 μM NIR QDs (right), in 100% FCS, as a function of excitation fluence rate and time. Note that the abscissa for IRDye78-CA is in seconds and that for NIR QDs is in minutes. (**e**) Fluorescence stability of 1 μM NIR QDs, in 100% FCS, at 37 °C over time.

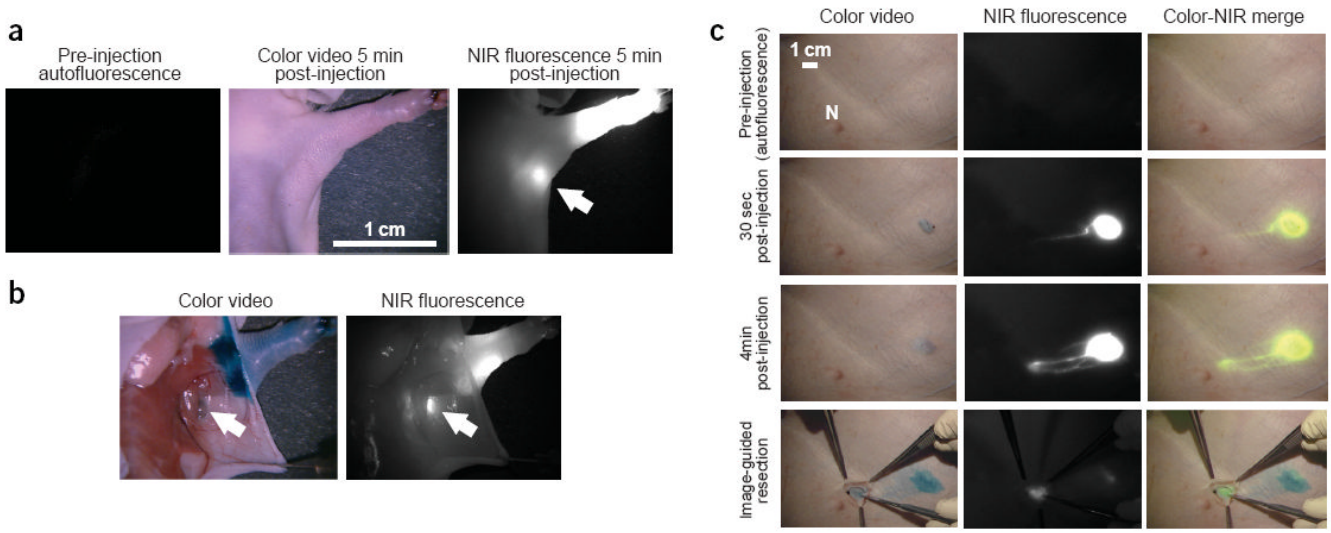

Figure 2.

NIR QD sentinel lymph node mapping in the mouse and pig. (**a**) Images of mouse injected intradermally with 10 pmol of NIR QDs in the left paw. Left, pre-injection NIR autofluorescence image; middle, 5 min post-injection white light color video image; right, 5 min post-injection NIR fluorescence image. An arrow indicates the putative axillary sentinel lymph node. Fluorescence images have identical exposure times and normalization. (**b**) Images of the mouse shown in **a** 5 min after reinjection with 1% isosulfan blue and exposure of the actual sentinel lymph node. Left, color video; right, NIR fluorescence images. Isosulfan blue and NIR QDs were localized in the same lymph node (arrows). (**c**) Images of the surgical field in a pig injected intradermally with 400 pmol of NIR QDs in the right groin. Four time points are shown from top to bottom: before injection (autofluorescence), 30 s after injection, 4 min after injection and during image-guided resection. For each time point, color video (left), NIR fluorescence (middle) and color-NIR merge (right) images are shown. Fluorescence images have identical exposure times and normalization. To create the merged image, the NIR fluorescence image was pseudocolored lime green and superimposed on the color video image. The position of a nipple (N) is indicated.

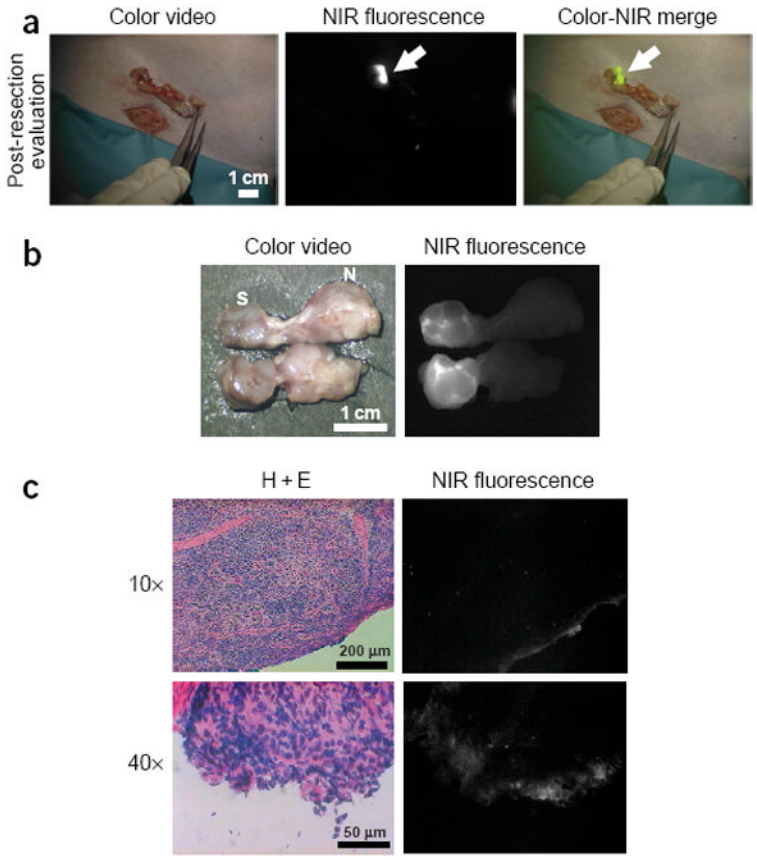

Figure 3.

Post-resection inspection of the surgical field and evaluation of NIR QD lymph node retention. (**a**) Post-resection evaluation of the surgical field. Shown are color video (left), NIR fluorescence (middle) and color-NIR merge (right) images. Arrows indicate the resected sentinel lymph node. (**b**) NIR QD retention by the resected SLN (S) and the next lymph node (N) in the chain is shown in this bisected specimen. (**c**) Histologic analysis of frozen sections of the SLN in **b**. Shown are two representative hematoxylin and eosin (H + E)-stained sections and consecutive unstained sections photographed on a NIR fluorescence microscope.